INVESTIGATIONS OF FRACTURE TRACE ANALYSES AND REMOTE SENSING APPLICATIONS IN SINGIDA REGION, TANZANIA

Senior Thesis

Submitted in partial fulfillment of the requirements for the

Bachelor of Science Degree

At The Ohio State University

By

Peter Gregory Gordineer

The Ohio State University

2019

Approved by

W.B. Lyons, Advisor
School of Earth Sciences

TABLE OF CONTENTS

ABSTRACT

Fracture trace analyses are historically proven methods of studying and predicting subsurface aquifer prevalence and flows within fractured bedrocks and are ultimately useful for producing target well drilling sites in areas of highly concentrated fracture traces. Recent advances in technology have allowed for greater access to high resolution satellite imagery datasets suitable for hydrogeologic use. Fracture trace analyses have been performed in part by taking advantage of these recent technological improvements, but none have completely removed the need for field measurements or aquifer pump tests.

In this study, the applications of remote sensing data towards fracture trace analyses have been examined within literature, and a process has been produced, tested, and iteratively improved in which fracture traces may be produced utilizing only remote sensing techniques.

This process is most applicable in test areas where field studies are unavailable or impractical, but existing satellite data are available for use. These situations are often met within humanitarian drilling projects in rural regions of Africa, such as those presented here.

Data comparisons of the results of this study show this process produces results similar to those found in existing literature. Similarly, the data suggest that this process can identify well target sites with potential for significant improvements in water output quantity, and that the concepts presented in this study merit further exploration.

ACKNOWLEDGEMENTS

Funding for this project came from The Coca-Cola Company and from USAID. I thank The Ohio State University Global Water Institute for the opportunity to participate in this project. I would also like to thank Dr. Audrey Sawyer for suggesting the initial ideas for this research and Jeffrey Melaragno and Rebecca Gianotti for providing guidance on site selection.

I would like to thank my advisor, Dr. Berry Lyons, for his assistance in the completion of this project.

I would also like to thank Dr. Anne Carey, as this project could never have been completed without her guidance and mentorship.

I would also like to thank Mike and Cindy Morgan for creating The School of Earth Sciences Field Experience Travel Fund, allowing my peers, Earth Sciences students of the future, and me to receive funding to attend field camp. Field camp through Ohio State provided us with valuable experiences, applying knowledge developed in a controlled classroom to real-world endeavors at small and large scales.

I would like to thank my peers throughout my time at Ohio State, for helping in many ways throughout my education. I would especially like to thank Bobby Murcko, Logan Fries, and Nicole Price for adding inspiration and enjoyment to my academic career.

I would like to thank my grandparents for their help and love along the way. I would like to thank my sister Samantha for always being there. I would of course also like to thank my amazing parents Susanne and Gregory Gordineer, for without their love and support I would not be in the position to write this today.

List of Figures

LIST OF TABLES

INTRODUCTION

Fractures are important hydrogeologic features that can increase the porosity and permeability of bedrock aquifers. Fractures provide fluid migration pathways and storage zones for groundwater in the subsurface and facilitate aquifer recharge (Seers & Hodgetts, 2016; Lattman & Parizek, 1964). Bedrock fractures form as a geomechanical response of the subsurface geology to crustal stresses, be they isotropic, normal, shear, or a combination (Seers & Hodgetts, 2016). Stresses result from a combination of tectonic, thermal, lithostatic and gravitational forces, as well as fluid potential gradients (Seers & Hodgetts, 2016).

By mapping fracture zones, or areas of closely spaced fractures within bedrock, hydrogeologists can identify areas of greater aquifer connectivity and target those sites for groundwater wells, a particularly useful exercise in areas with low primary porosity of the bedrock (Seers & Hodgetts, 2016).

Fracture trace mapping involves identifying surficial expressions of sub-surface bedrock fracture zones. Fracture traces are linear to sub-linear features, often indicated by surface features such as stream alignments, vegetation lineaments, and surface depressions (Lattman & Parizek, 1964). Wells located on surface manifestations of bedrock fractures, especially the intersections of multiple fracture traces within a fracture trace zone, have been shown to have higher water yields in some aquifers (Lattman & Parizek, 1964; Seers & Hodgetts, 2016; Brook et al. 1986). It has been shown that these intersections occur in correlation with zones of high secondary permeability (Brook et al., 1986). Fracture trace mapping is therefore an efficient way to increase the likelihood of drilling high-yield wells in bedrock aquifers.

The literature suggests that fracture trace intersections, having higher secondary permeability and transmissivity than that of average bedrock areas, produce measurably altered groundwater chemical levels due to relatively high rates of rock-water interaction (Satyanarayana et al., 2007).

Fracture trace mapping is performed by analyzing aerial images for surficial fracture features and then ground-truthing mapped features in the field. Features such as recent sedimentary deposits, roads or other human disturbances, and flooding washouts can mask fracture traces or make their identification challenging (Thiele et al., 2017; Lattman & Parizek, 1964). Fractures can be particularly difficult to map in agriculturally dense regions, where large soil deposits are continually disturbed over relatively short intervals of geologic time. Within these agricultural regions, however, it is possible to identify indirect evidence of features following the path of fracture traces. For example, soil drying rates post-till may create aerially visible changes in soil moisture near fracture zones (Lattman & Parizek, 1964). To combat some of these potential challenges, fracture trace mapping can sometimes be performed preemptively, identifying potential well sites before agricultural development, then referencing back to this data post-development as necessary.

Typically, fracture trace mapping has been performed using stereoscopic imagery representing a three-dimensional view of the target region (Lattman & Parizek, 1964; Seers & Hodgetts, 2016). Stereoscopic images may not be available or may not be accessible for the applications of certain projects, but the availability of publicly available high-resolution aerial images has dramatically increased across the globe in recent years. Modern techniques of fracture trace mapping do not differ significantly from those of the past; however, computer-

aided mapping technologies have facilitated the process. These techniques have been developed to be both more efficient and more effective at correctly identifying fracture traces from data sources (Seers & Hodgetts, 2016). For example, modern photo manipulation and edge detection techniques can be applied to high-resolution two-dimensional satellite imagery to produce a normalized color gradient. This processing technique helps detect gradational, subtle changes typical of surficial fracture trace manifestations (Thiele et al., 2017).

While fracture trace mapping has been proven to be effective at well-siting in aquifers in areas of the world such as central Pennsylvania (Lattman & Parizek, 1964) and northern England (Seers & Hodgetts, 2016), there has been no rigorous testing of these methods upon bedrocks in the surrounding regions of major rifting zones, such as those present in Tanzania. Tanzania is dominated by low-productivity igneous and metamorphic bedrock aquifers (MacDonald & Tyler-Whittle, 2002). Identification of drilling sites is challenging, and multiple dry boreholes are often drilled before reaching water. Geologic consulting firms are hired to perform fracture trace analysis as part of initial reconnaissance assessments before drilling begins to minimize the risk of dry holes in parts of Tanzania. However, these fracture trace analyses do not always include ground-truthing surveys. Here, I produce an aerial fracture trace analysis for the targeting of drill sites in the Singida Region of Tanzania. In particular, I examine the challenges of conducting fracture trace analysis when ground-truthing is not possible.

BACKGROUND

Prior Hydrogeologic Investigations

Previous work in the region by Sangea et al., (2016) showed the predominant aquifer systems of Tanzania and their associated average productivity (Figure 1). The region targeted for this analysis exists in an area dominated by basement aquifers.

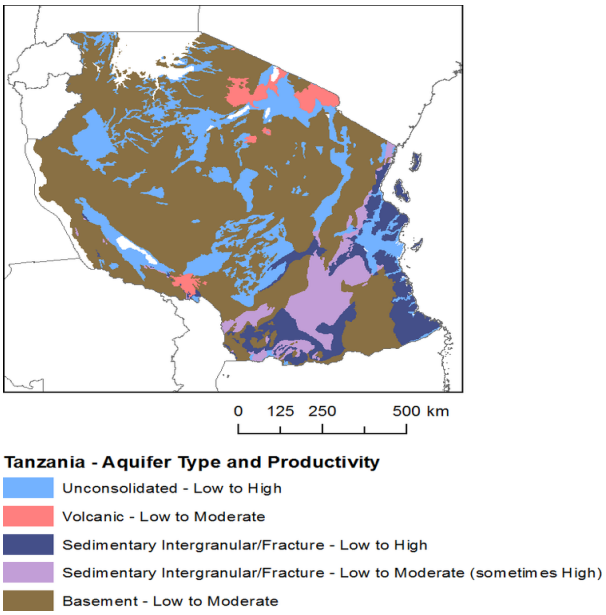

Figure 1. Map of Tanzania showing aquifer type and productivity (Sangea et al., 2016). The study area within Singida extends through both basement and unconsolidated aquifers, of varying productivity ranges.

The current assessment has been conducted in two parts. The initial assessment centered around four known boreholes. The primary goal of this initial assessment was to develop a process that could be applied to future regions without known boreholes. The first borehole site was drilled in close proximity to Mtinko, and found to have highly saline water, unsuitable for domestic use. The second borehole site, also outside of Mtinko, was flooded and abandoned, with no data given. The third borehole site was drilled in close proximity to Tutu, and was found to have highly saline water, also not recommended for domestic use. The fourth borehole site, the final site outside of Mtinko, was found to produce domestically viable water.

Second, a fracture trace analysis was performed for five villages that have not yet been drilled but are expected to be drilled in the future. These villages have had water quality tests. These villages are Majiri, Mdilu, Msange, Ngimu, and Mvae respectively. Majiri and Mvae have existing wells in place with low water quality. Each of these sites exhibit nitrate NO_3 values beyond the 1996) Organization (WHO) acceptable range, values of 328 and 70 mg/l respectively, with the WHO acceptable limit of 45mg/l (WHO, 1996). Mvae also exhibits fluoride values of 2.26 mg/l, greater than the WHO acceptable limit of 1.5mg/l. Msange and Ngimu have existing wells in place with both low water quality and low yield. Ngimu exhibits nitrate NO_3 values of 70mg/l, beyond the WHO acceptable limit of 45mg/l. Msange exhibits fluoride values of 2.97 mg/l, beyond the WHO acceptable limit of 1.5mg/l. Mdilu has an existing well with acceptable yields and water quality, with low total dissolved solids and acceptable nitrate levels (United Republic of Tanzania, 2019).

Regional Geology

The drill target area consists of generally flat terrain in the semi-arid Singida Region of Tanzania. The surveyed area exhibits an average elevation of about 4200m, with hills and slopes upwards of 200-300m variation (United Republic of Tanzania, 2019). This region experiences low levels of precipitation, at maximum of 1450mm/year, lower than expected evapotranspiration, leading to unsustainable surface water bodies (United Republic of Tanzania, 2019).

Singida lies on the Tanzania Craton (Figure 2) (Sangea et al., 2016), which divides the East African Rift. The surface geology of the region consists primarily of gray-red sandy soils, formed during the Neogene, overlying the basement rock beneath (United Republic of Tanzania, 2019). Key geologic features of Singida and surrounding regions also include a Precambrian orogenic belt (Figure 2). The basement rock is characterized by the Dodoman System of interlayered basement bedrock, formed during the Archean. This bedrock is dominated by coarse grained granites, gneisses, and schists, all of which are intruded by various pegmatic and dolerite dykes. The fractures within the 2 billion year old bedrock, as well as the intruding dykes, improve the yield of potential groundwater wells when intersected.

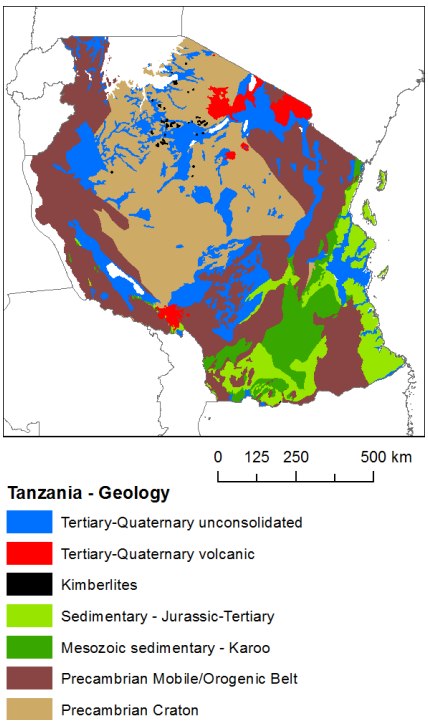

Figure 2. Map of Tanzania showing most prominent lithology of each region of Tanzania (Sangea et al., 2016). The study area of Singida extends through the Precambrian craton, and Tertiary-Quaternary unconsolidated deposits.

METHODS

Satellite Data Acquisition

Site coordinates for the target villages were provided by Maji Tech Drilling Co. LTD as part of the Mughanga Pilot Project commissioned by Ohio State University's Global Water Institute. For each of these initial target areas, satellite data were collected over a 1.3 by 2 kilometer rectangle centered on the target.

Following this initial test on four known villages, this process was applied to larger spatial scales. The recommended search area of each target, after discussion and desire to meet needs of industry standards, was expanded to concentric circles of increasing 0.5km radii, with an approximately 3-kilometer radius. These study areas are similar in scale to those performed in other analyses using this method (Brook et al., 1986). This updated process was applied to five new village target locations. Satellite imagery were obtained from the Google Earth satellite imagery dataset, available from Google.

Data Processing and Interpretation in QGIS

Software-aided analysis was performed using the open source QGIS software program according to the methods of Seers and Hodgetts (2016) and Thiele et al. (2017). Briefly, the Google Earth satellite imagery dataset was imported into QGIS and then exported as a high-resolution PNG raster file for the area centered on each site, with kilometer-scale radii overlain (Figure 3a). Next, the raster file for each area was imported and split into a single color-band image using a QGIS raster calculation. This black and white image was simply a wide band grayscale version of the original satellite imagery (Figure 3b). The grayscale image was then processed through the QGIS GeoTrace plugin using a Sobel vertical transformation, a derivative of the Sobel edge detection method. GeoTrace produces a GeoTiff output file of detected edges (Figure 3.c.), viewable in QGIS.

With these Sobel files, fracture traces were mapped using the least-cost lineament calculation method (Figure 3.d) following the work of Thiele et al. (2017). This approach traces sublinear gradational boundaries. I identified and removed "pseudo-traces," or linear features that were unlikely to be representative of fracture traces (blue traces in Figure 3d). I interpreted pseudo-traces based on aerial images, ruling out features that followed roads, agricultural edges, and streams. The need to rule out pseudo-traces is a drawback of utilizing the Sobel edge detection methods and possibly a weakness of using non-stereoscopic mapping techniques. The remaining fractures (red traces in Figure 3d) are interpreted as possible fracture traces that would be ground-truthed if possible. These fracture traces have been recorded in figures 4 through 7 for the initial four target areas, and figures 8 through 12 for the following five areas.

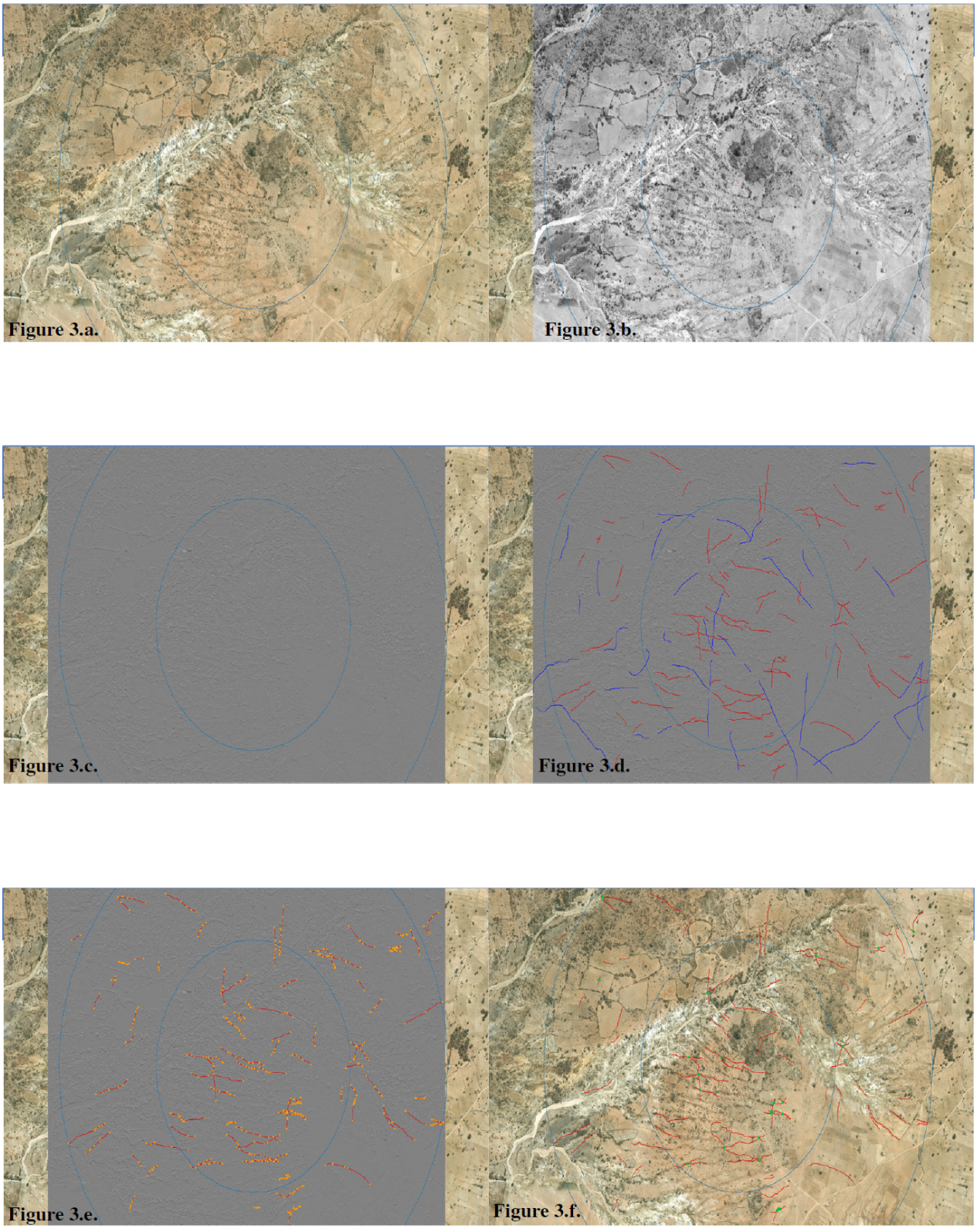

Figure 3. Map of test area showing progressive steps taken throughout data processing, with key datasets overlain.

Geospatial Analysis using GeoTrace

In the absence of ground-truthing, I performed some basic geospatial analysis to identify fracture trace orientations. Geologic processes in an extensional tectonic setting should yield sets of predominant fracture orientations. I used orientation information to improve selection of most likely fracture traces. Specifically, I determined the endpoints of potential fracture traces using the QGIS field calculator within the attribute tables (Figure 3e). The average azimuthal orientation of each fracture trace was then calculated as the strike and mapped on a standard rose diagram for each target area. Biases can influence the resulting rose diagrams, included user preferential identification of horizontal edges, negative aspects of using vertical Sobel transformations, agricultural growth patterns, property boundaries, road orientations, and property boundaries. I compared the rose diagrams with structural maps (Sangea et al., 2016) to interpret the most likely orientations associated with true fracture traces.

Post-Processing and Drill Target Identification

Following azimuthal orientation calculations, I mapped the intersections of fault traces (green points in Figure 3f). I then scrutinized all points to determine relative potential for a successful well. In my interpretation, I selected for intersections of features that showed substantial geologic and surficial evidence of fracture trace zones, outlined above and by Lattman & Parizek (1964). Specifically, I looked for evidence of topographic sags, linear drainages, natural agricultural gradients, and other hydrogeologic factors. I identified locations where many or all intersecting fault traces had strong positive indicators for being accurately identified as areas for high potential of success, or “drilling targets.”

RESULTS

Data Review

Drill target areas exhibit variations in terrain and surface features. There exist areas of high contrast associated with lightly colored surficial soils as well as higher brightness satellite imagery (Figure 6). Cloud cover and existing surface water bodies create areas where data cannot be processed (Figure 8). Dense forest cover (Figure 11) also creates areas of missing data. Large changes in elevation (Figures 11 and 12) seem to provide potential for higher quantity of discernible data points.

Use of a relatively small-scale test area during initial tests allowed for minor terrain features to be observed. Change of scale (From Figures 7 to 8) allowed greater impact of large-scale geologic features, and created a system of pre-filtering, whereby increased area and constant relative resolution caused man-made linear features and small-scale drainages to become less prominent (Figure 11).

The initial four tests sites resulted in an average of 18 useful fracture trace intersections. The further five drill target sites resulted in an average of 34.8 fracture trace intersections. Removal of the Majiri site (Figure 8), with much of its area consisting of surface water features, increases the average to 41. From the initial testing to the second set of test sites, the test area of each site increases in size from approximately 7 km^2 to 28 km^2. The increase in area by a factor of 4 created an average increase in data points by a factor of about 2.3. This is a notable change in average data points per unit area.

Assessment of Previously Drilled Villages

Use of available borehole data for the initial four test sites allows for comparison of the test methods to real results. The first borehole site, found to have highly saline water, had a single fracture trace within 100m of the drilled well. However, no intersecting fracture traces were located within 400m of the borehole (Figure 4). The second borehole site lacks available data for comparison (Figure 5). The third borehole site features a well with highly saline water. The data presented (Figure 6) show multiple fracture traces within 100m, a single fracture trace intersection within 150m, and numerous within 500m. The fourth borehole site features a well which produced domestically viable water. This site is directly intersected by a recorded fracture trace. In addition, a large cluster of numerous fracture trace intersections is found within 500m to the northeast (Figure 7).

Assessment of Villages Yet to Be Drilled

Comparison of the following five test sites to available borehole data is also possible. Of the five, the site at Mdilu (Figure 9) is the only site with a well producing water with acceptable quality and yield. The Mdilu site index 12 location (Table 1 in Appendix) is the only experience of direct overlap of available well data and projected drill target location at a fracture trace intersection based on the data presented. The sites at Majiri, Ngimu, and Mvae (Figures 8, 11, 12) exhibit fracture traces within 100m of their respective borehole locations, with Ngimu and Mvae experiencing fracture trace intersections within 300m of the borehole site. The borehole site at Majiri was just within 1500m of the nearest fracture trace intersection presented in this dataset (Figure 8). The borehole site at Msange experiences no fracture traces within 150m,

however three fracture trace intersections occur within the range of 400m–500m distance to the Northwest (Figure 10).

Several factors complicate the interpretation of fracture traces from aerial images. Generally, the terrain in Singida exhibits variations in surface features and high contrast areas associated with changes in surface soils (Figure 6). Additionally, tiled satellite images differ in brightness, which can lead to artificial boundaries of high contrast. Cloud cover and existing surface water bodies create areas where data cannot be recorded (Right of Figure 8). Dense forest cover (Lower Figure 11) also creates areas of missing data. Large changes in elevation (Figures 11 and 12) provide potential for higher quantity of discernible data points.

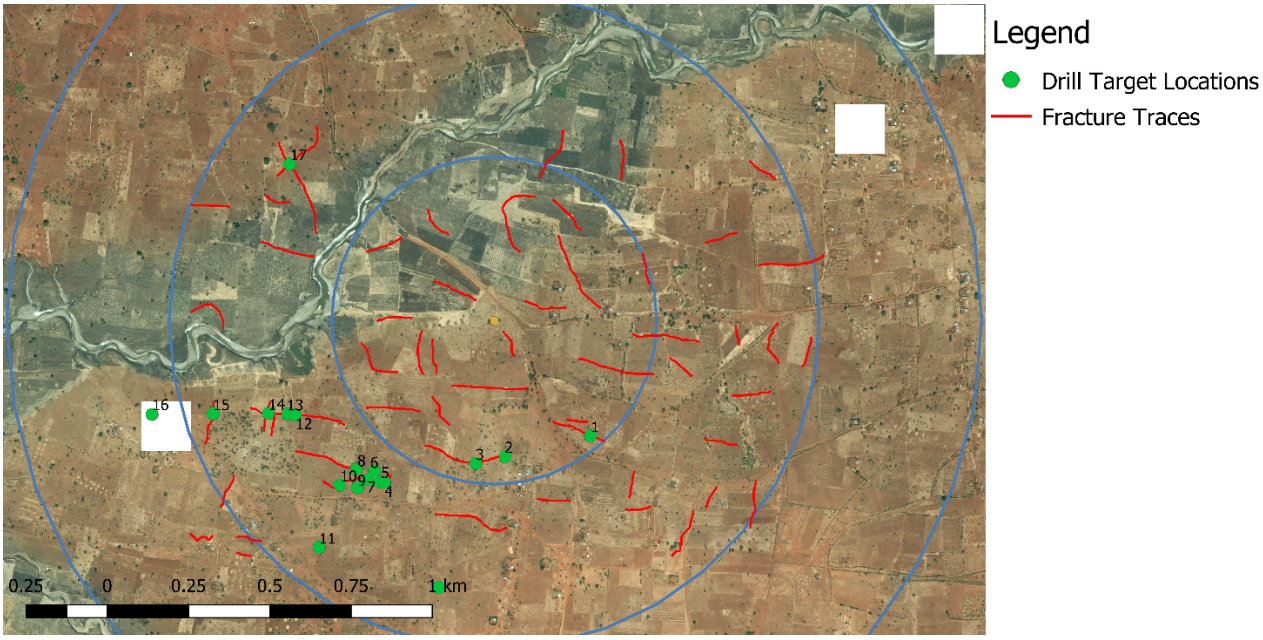

Figure 4. Focused satellite view upon borehole site 1, provided by Mughanga Pilot Project team. Blue circles shown at 0.5-kilometer radii intervals. Coordinates have been provided for these locations in Table 1, referenced to the location 1, and the numbering system above.

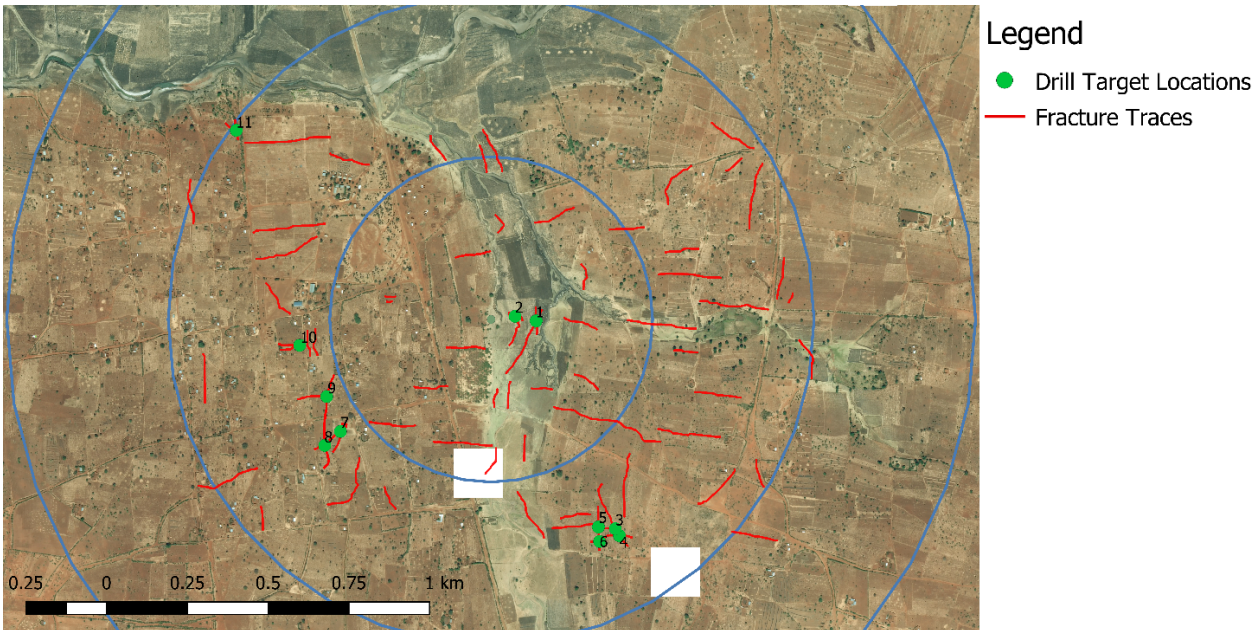

Figure 5. Focused satellite view upon borehole site 2, provided by Mughanga Pilot Project team. Blue circles shown at 0.5-kilometer radii intervals. Coordinates have been provided for these locations in Table 1, referenced to the location 2, and the numbering system above.

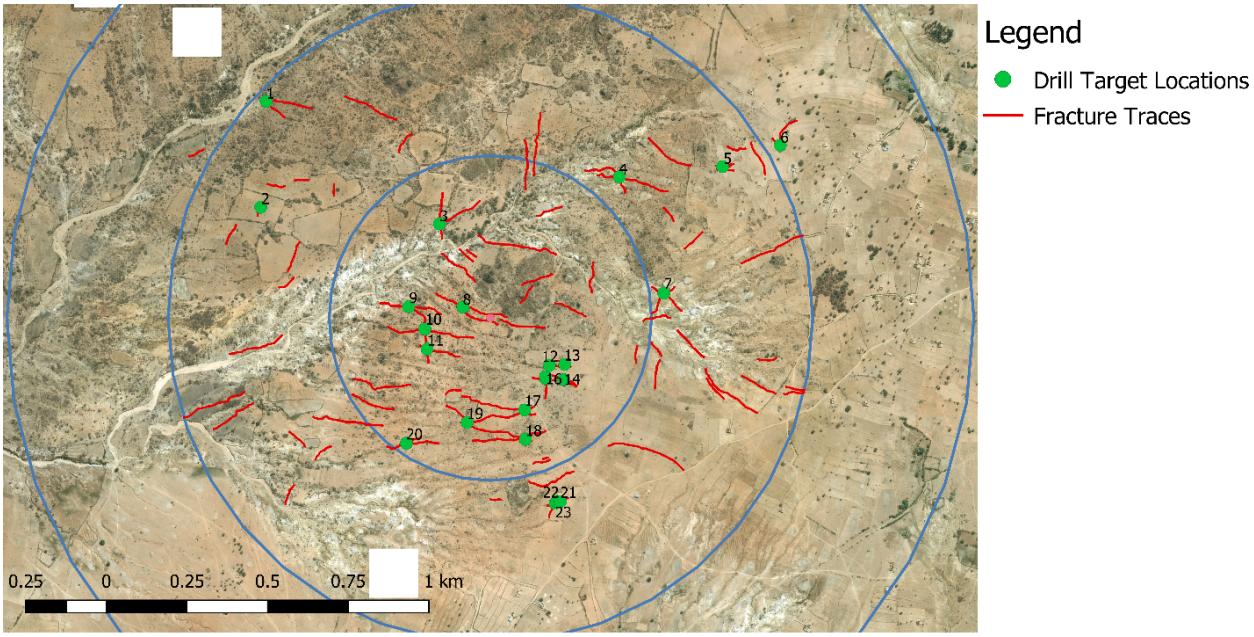

Figure 6. Focused satellite view upon borehole site 3, provided by Mughanga Pilot Project team. Blue circles shown at 0.5-kilometer radii intervals. Coordinates have been provided for these locations in Table 1, referenced to the location 3, and the numbering system above.

.

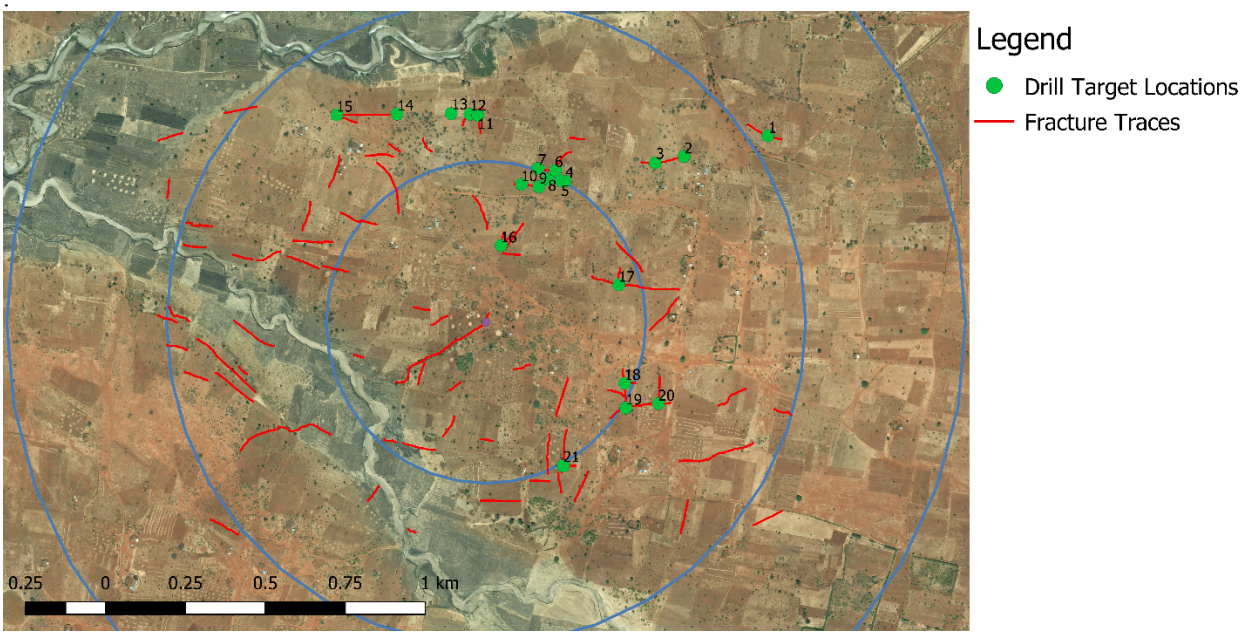

Figure 7. Focused satellite view upon borehole site 4, provided by Mughanga Pilot Project team. Blue circles shown at 0.5-kilometer radii intervals. Coordinates have been provided for these locations in Table 1, referenced to the location 4, and the numbering system above.

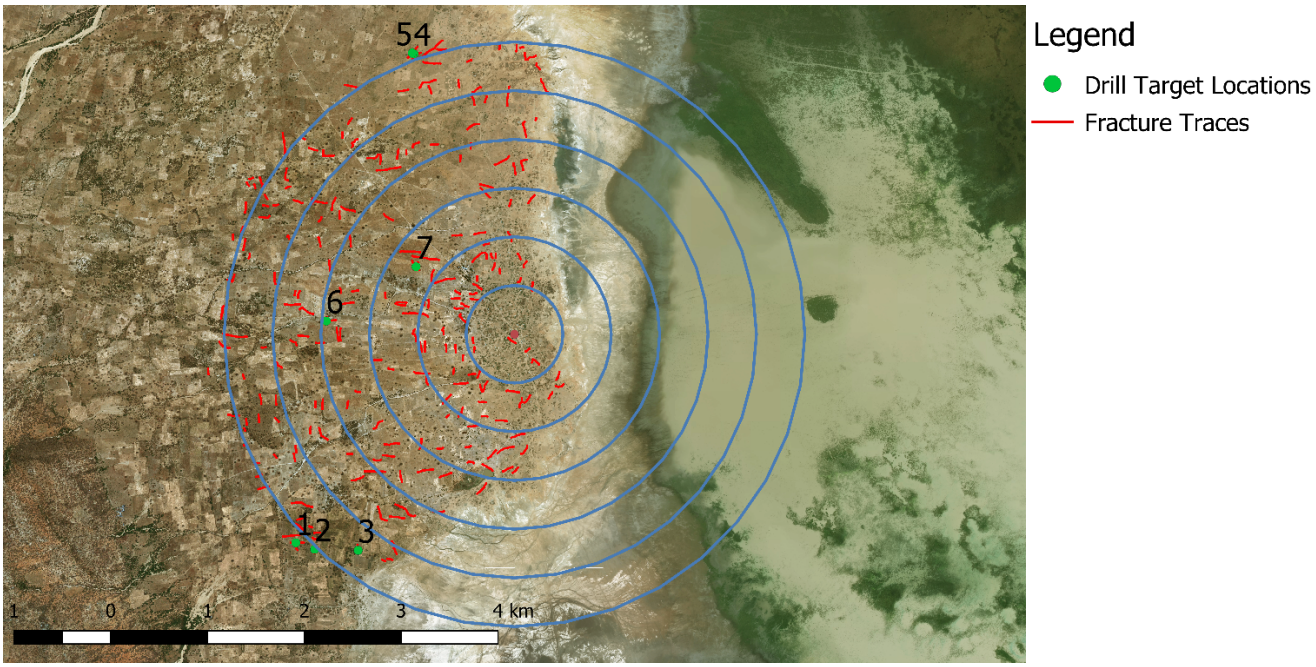

Figure 8. Focused satellite view upon Majiri. Blue circles shown at 0.5-kilometer radii intervals. Coordinates have been provided for these locations in Table 1, referenced to the location Majiri, and the numbering system above.

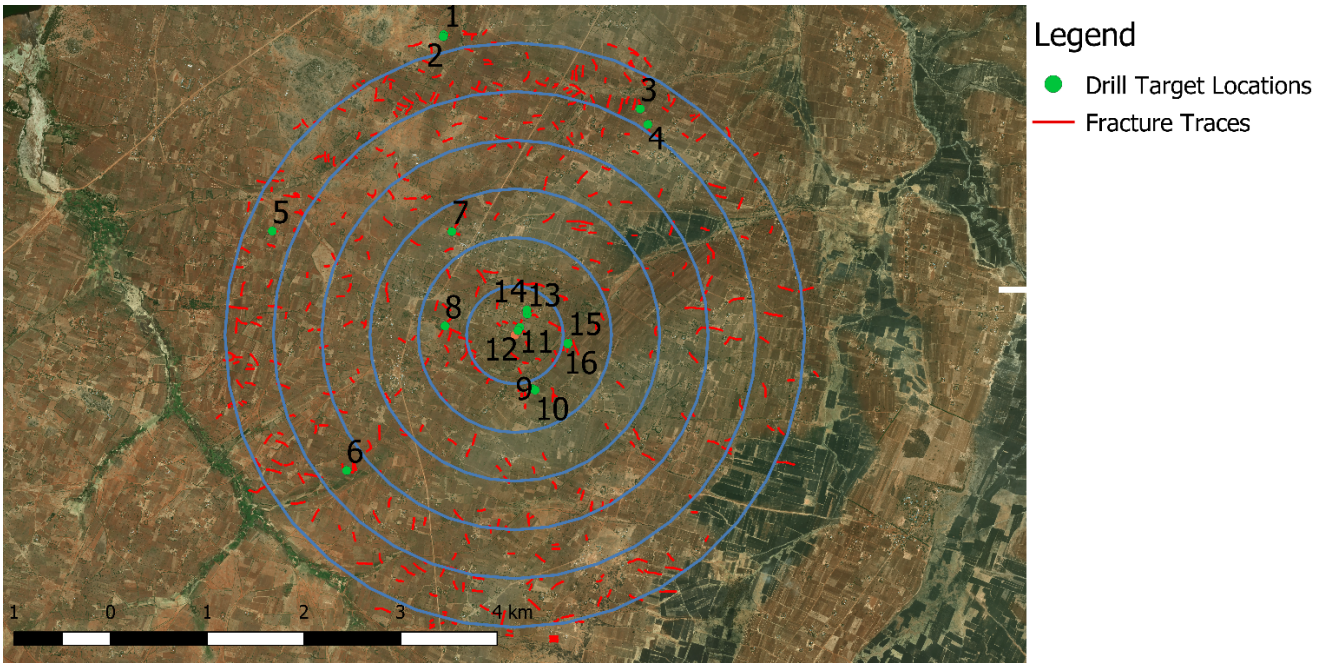

Figure 9. Focused satellite view upon Mdilu. Blue circles shown at 0.5-kilometer radii intervals. Coordinates have been provided for these locations in Table 1, referenced to the location Mdilu, and the numbering system above

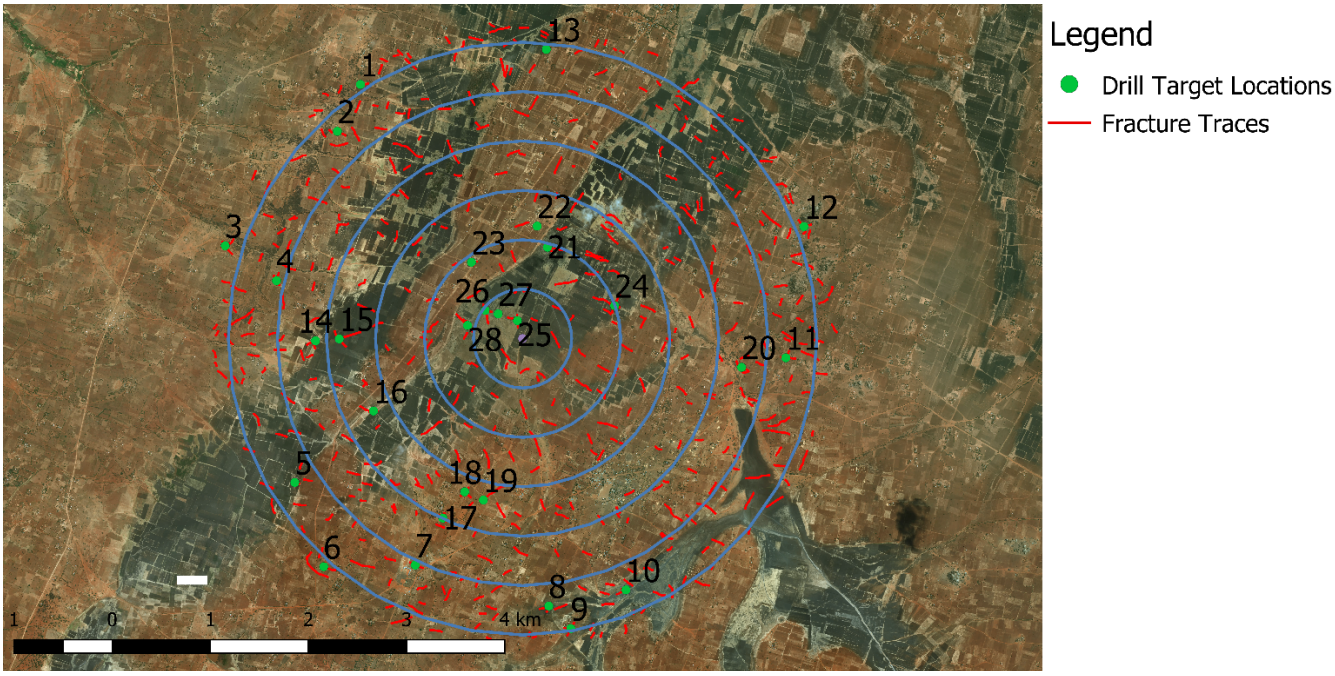

Figure 10. Focused satellite view upon Msange. Blue circles shown at 0.5-kilometer radii intervals. Coordinates have been provided for these locations in Table 1, referenced to the location Msange, and the numbering system above

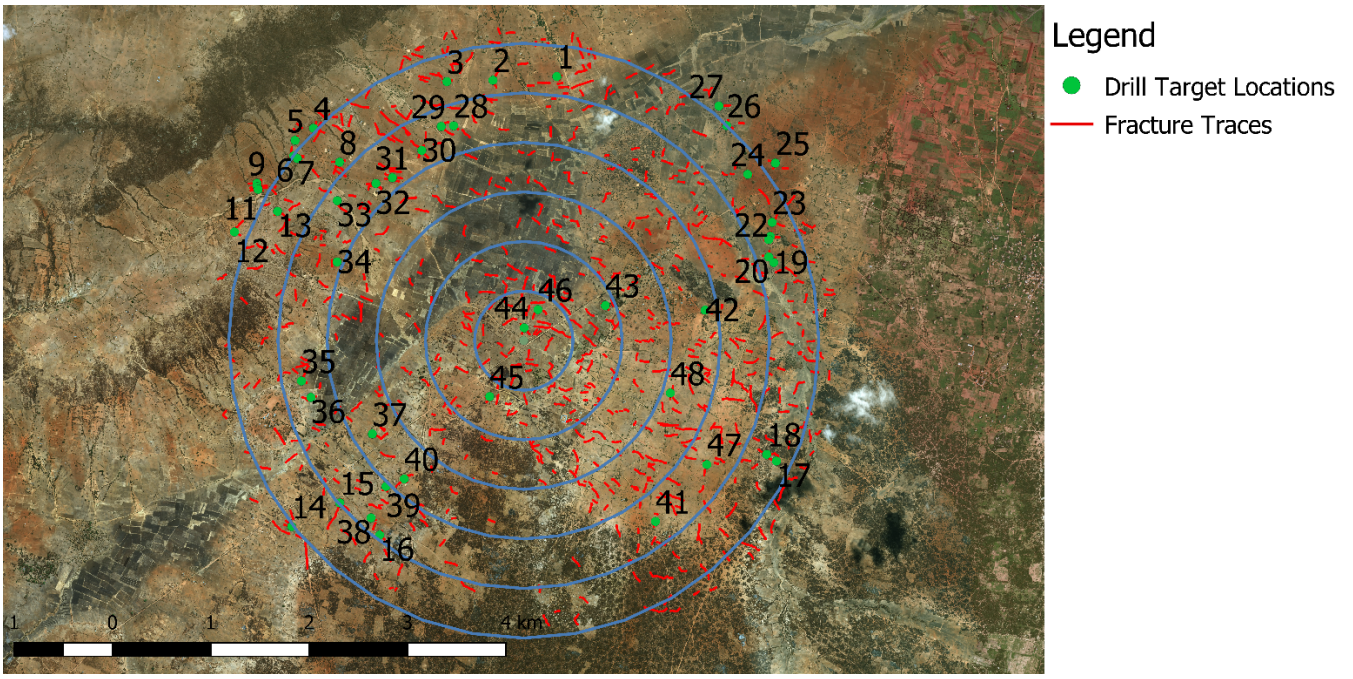

Figure 11. Focused satellite view upon Ngimu. Blue circles shown at 0.5-kilometer radii intervals. Coordinates have been provided for these locations in Table 1, referenced to the location Ngimu, and the numbering system above

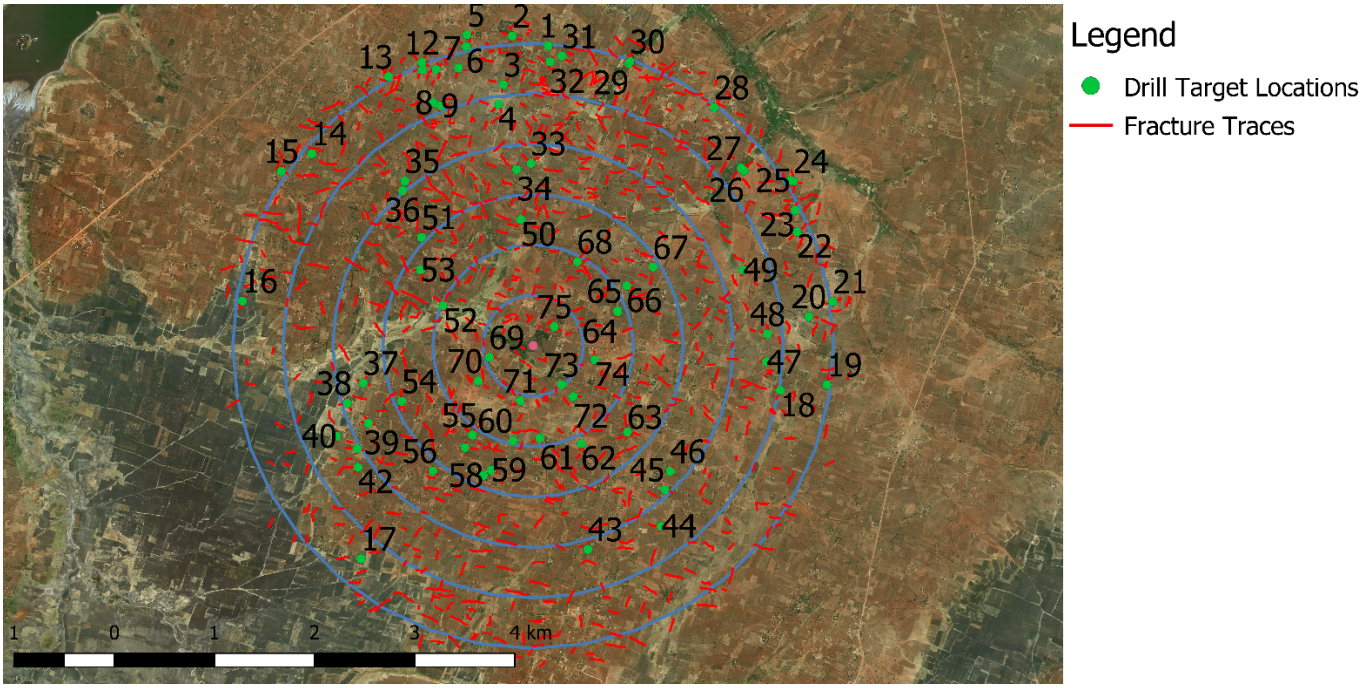

Figure 12. Focused satellite view upon Mvae. Blue circles shown at 0.5-kilometer radii intervals. Coordinates have been provided for these locations in Table 1, referenced to the location Mvae, and the numbering system above.

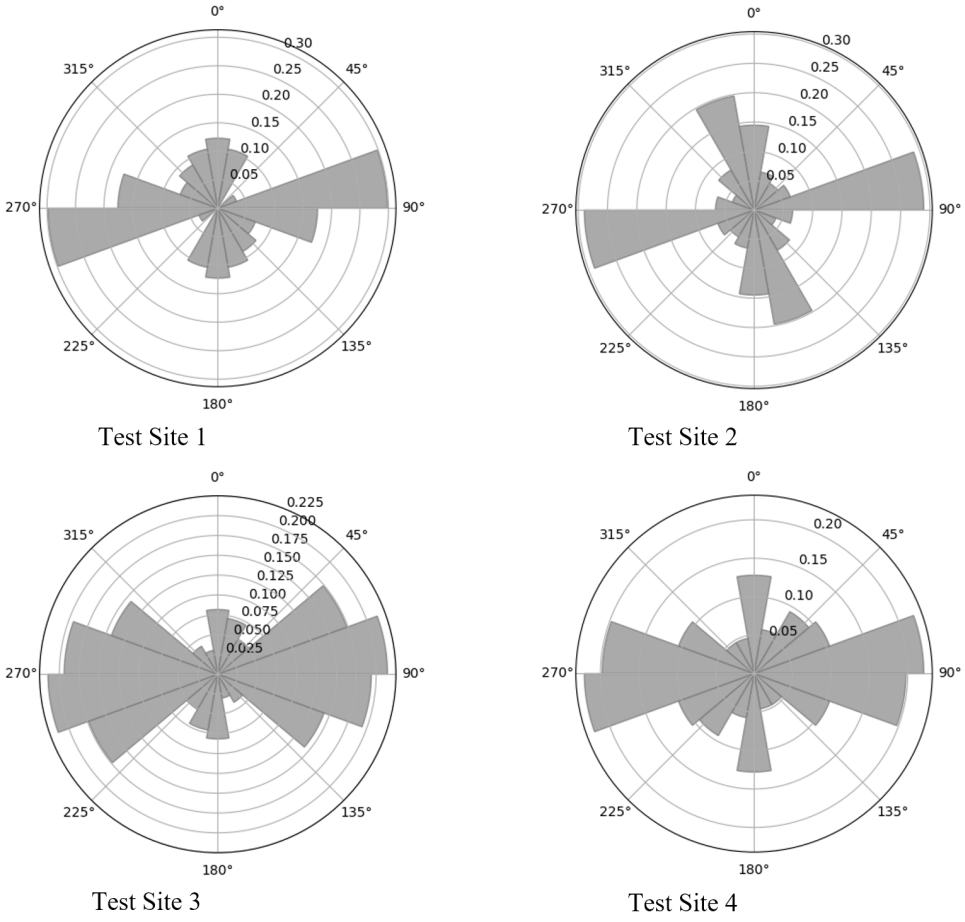

Figure 13. Rose diagrams of orientation data of fracture traces for initial four test sites. Produced using QGIS GeoTrace tool, by calculating linear azimuth between endpoints of each fracture trace. Each of the test sites shows a major trend of East-West horizontal fracture traces.

Discussion

To assess the influence of extent and scale on this analysis, I compared an analysis of the initial test areas with extent of 7 sq. km to the secondary tests of 28 sq. km (Figures 4–7 and 8–12 respectively). Use of relatively small-scale test areas allowed for less major terrain features to be observed. Expansion of the scale (From Figures 4 to 5) resolved the impact of large-scale geologic features and created a sort of pre-filtering, whereby increased area and constant relative resolution caused man-made lineations and small-scale drainages to become less prominent (Figure 8). The increase in area by a factor of 4 created an average increase in data by a factor of about 2.3. This is a notable change in average points per unit area. With these assessments being performed in different areas, it cannot be determined whether that the decrease in average data points per area is due only to change in scale, as these areas contain different geology, and thus a different number of fractures to be identified (Berkowitz et al., 2000). It is notable that historical study areas utilize similar 0.5km radii to perform their analysis, such as those presented by Brook et al. (1986).

Comparison of the results of these tests to similar tests in published literature, such as those by Lin et al. (2014), yield promising results. The tests performed by Lin et al. (2014) were made within sandstone structures of South Africa, but the process itself is directly comparable to the process performed in this work. Comparison of the rose diagrams produced herein at the initial 4 test sites (Figure 13) to those produced by Lin et al. (2014) (Figure 14) produce similar results. The similarities between the data of test site 2 and the study of Lin et al. (2014) are particularly interesting, as they are most similar. A comparison of the data at the sites of Lin et al. (2014) to those performed in this study suggests that there is no reason that horizontal East-West orientations should dominate these regions.

Figure 14. Rose diagrams of orientation data of fracture traces for Lin's test area in South Africa (Lin et al., 2014). Direct comparison of these data in literature can be made to the experimental data presented here.

Initial comparison to the test by Lin et al. (2014) shows similar small fractures generated, but with much more consistency in azimuth orientation than those measured in this analysis. This is certainly due in part to these fractures being mapped by hand-measurements of azimuthal data in the field, the fractures traces presented here are projections solely based upon satellite data, which are expectedly less accurate than field data. The fracture trace networks produced by Lin et al. (2014) were made utilizing pump test data.

Observation of the hydrogeochemical changes surrounding the measured fracture trace intersections yields interesting results. The well at Mdilu meets water quality standards for chemical concentrations of nitrate, fluoride, and total salt. This well at Mdilu occurs directly upon a fracture trace intersection. Ngimu and Mvae both have existing wells at a distance of approximately 300m from a fracture trace intersection, and both exhibit high nitrate levels. Msange and Ngimu both exhibit fracture trace intersections within 400m of the current borehole site, and both exhibit high fluoride levels. Pump tests could be conducted in future work to determine whether these fracture trace intersections may be influencing groundwater chemical changes. Results of other previous explorations into geochemical correlations with fracture trace intersections have shown to have correlative effect (Satyanarayana et al., 2007).

CONCLUSIONS

This study has shown that the method used has been successful at identifying at least one useful and productive well target location, shown at Mdilu (Figure 6). This study has produced results that are in many ways comparable to historical studies, and has in itself identified improvements that can be made upon its process. The results of this study show that remote sensing applications towards fracture trace analyses merit further study, further exploration and refinement.

SUGGESTIONS FOR FUTURE RESEARCH

Multiple areas for future research exist. First, an important area for future research is to obtain ground truth for a set of identified fracture traces with data obtained from satellite images and directly apply field data measurements. This will allow for direct comparison of the presented remote sensing methods to proven field methods. Structural surveys are needed for ground truthing. It is possible that application of ground truthing over limited areas, combined with a statistical analysis of trend data on fracture trace orientations could prove useful for interpreting fracture traces in other regions.

Second, a clear need has been established to assess whether fracture trace analysis can improve the probability of higher well yields in certain groundwater aquifer systems of rural Tanzania. If dry or low-yielding wells are drilled, future research could be conducted to determine why these failures occur, and efforts should be made to modify the approach of this type of fracture trace analysis to be more accurate under differing geologic circumstances.

Third, an assessment of the impact of scale on remote fracture trace analyses could be made by performing multiple analyses at different spatial scales upon the same region. There may be a scale best suitable for this analysis, however testing has yet to be done to determine this.

Finally, it is a near certainty that an experienced hydrogeologist could produce more accurate results when taking direct measurements in the field, or when utilizing higher resolution and more advanced datasets. These datasets may include 3-Dimensional trace maps from Lidar surveying (Seers & Hodgetts, 2016), high resolution topographic and structural maps (Lattman & Parizek, 1964), or in-depth borehole comparison throughout a target area (Lattman & Parizek, 1964). A method of future research could be to apply the presented 2-dimensional satellite fracture trace mapping and compare to 3-dimensional fracture trace mapping within the same testing area.

REFERENCES CITED

Berkowitz, B., Bour, O., Davy, P., & Odling, N. (2000) Scaling of fracture connectivity in geological formations. Geophysical Research Letters. 27(14). 2061-2064.

Brook, G. A., Carver, R., & Sun, C.-H. (1986) Predicting Well Productivity Using Principal Components Analysis. Professional Geographer. 38(4). 324-331.

Google Earth Dataset for Singida, Tanzania. *Google Earth, DigitalGlobe* (2018) http://www.earth.google.com [2019].

World Health Organization (1996) Guidelines for drinking-water quality, 2nd ed. Vol. 2. Health criteria and other supporting information., Geneva, 1996.

Lattman, L.H. & Parizek, R.R. (1964) Relationship between fracture traces and the occurrence of ground water in carbonate rocks. Journal of Hydrology. 2. 73-91. 10.1016/0022 1694(64)90019-8.

Lin, L., Lin, H., & Xu, Y. (2014) Characterization of fracture network and groundwater preferential flow path in the Table Mountain Group (TMG) sandstones, South Africa. *Water SA*, *40*(2), 263-272.

MacDonald, A.M. & Tyler-Whittle, R.A. (2002) Minimizing fluoride in drinking water: fieldwork in Tanzania, August 2002. British Geological Survey Internal Report.

Thiele, S. T., Grose, L., Samsu, A., Micklethwaite, S., Vollgger, S. A., & Cruden, A. R. (2017) Rapid, semi-automatic fracture and contact mapping for point clouds, images and geophysical data, Solid Earth, 8, 1241-1253, https://doi.org/10.5194/se-8-1241-2017.

Sangea, H., Upton K., Dochartaigh B.É., & Bellwood-Howard, I. (2016). Africa Groundwater Atlas: Hydrogeology of Tanzania. British Geological Survey.

Satyanarayana, M. & Saad Al Hussin, M. (2007) Assessment of Groundwater Quality in a Structurally Deformed Granitic Terrain in Hyderabad, India. Environ. Monit. Assess. 131:117127. 10.1007/s10661-006-9461-9.

Seers, T. D. & Hodgetts, D. (2016) Extraction of three-dimensional fracture trace maps from calibrated image sequences. Geosphere, 12(4):1323–1340. doi:https://doi.org/10.1130/GES01276.1

United Republic of Tanzania (2019) *Water Sample Analytical Results*, Directorate of Rural Water Supply, Ministry of Water and Irrigation.

APPENDIX

Table 1.

List of coordinates of intersecting fracture traces at each of the following five testing sites: Majiri, Mdilu, Msange, Ngimu, Mvae. Followed by list of intersecting fracture trace coordinates at the initial four testing sites, with nearest village applied to naming scheme.

Village	Map Index #	Lat, Long (Dec. Degrees)
Majiri	1	-6.075343, 34.998486
Majiri	2	-6.075960, 35.000239
Majiri	3	-6.076050, 35.004298
Majiri	4	-6.029974, 35.009507
Majiri	5	-6.029905, 35.009356
Majiri	6	-6.054774, 35.001335
Majiri	7	-6.049735, 35.009710
Mdilu	1	-4.563424, 34.997380
Mdilu	2	-4.563609, 34.997345
Mdilu	3	-4.570316, 35.015700
Mdilu	4	-4.571756, 35.016406
Mdilu	5	-4.581646, 34.981387
Mdilu	6	-4.603860, 34.988312
Mdilu	7	-4.581692, 34.998132
Mdilu	8	-4.590453, 34.997489
Mdilu	9	-4.596282, 35.005665
Mdilu	10	-4.596404, 35.005897
Mdilu	11	-4.590586, 35.004461
Mdilu	12	-4.590873, 35.004303
Mdilu	13	-4.589351, 35.005150
Mdilu	14	-4.588980, 35.005127
Mdilu	15	-4.592029, 35.008960
Mdilu	16	-4.592113, 35.008952
Msange	1	-4.615504, 35.013776
Msange	2	-4.619799, 35.011657
Msange	3	-4.630268, 35.001348
Msange	4	-4.633463, 35.006060
Msange	5	-4.651924, 35.007742
Msange	6	-4.659634, 35.010394
Msange	7	-4.659490, 35.018808
Msange	8	-4.663230, 35.031066
Msange	9	-4.665312, 35.033067
Msange	10	-4.661752, 35.038168
Msange	11	-4.640520, 35.052836
Msange	12	-4.628505, 35.054494

Msange	13	-4.612304, 35.030838
Msange	14	-4.638959, 35.009643
Msange	15	-4.638790, 35.011823
Msange	16	-4.645384, 35.014969
Msange	17	-4.655204, 35.021324
Msange	18	-4.652788, 35.023341
Msange	19	-4.653536, 35.025056
Msange	20	-4.641387, 35.048790
Msange	21	-4.630403, 35.030952
Msange	22	-4.628467, 35.030007
Msange	23	-4.631771, 35.023972
Msange	24	-4.635724, 35.037141
Msange	25	-4.637104, 35.028186
Msange	26	-4.636171, 35.025215
Msange	27	-4.636501, 35.026420
Msange	28	-4.637555, 35.023605
Ngimu	1	-4.735410, 35.078743
Ngimu	2	-4.735736, 35.072891
Ngimu	3	-4.735854, 35.068700
Ngimu	4	-4.740120, 35.056433
Ngimu	5	-4.741229, 35.054751
Ngimu	6	-4.742642, 35.054640
Ngimu	7	-4.742898, 35.054973
Ngimu	8	-4.743216, 35.058817
Ngimu	9	-4.745121, 35.051269
Ngimu	10	-4.745481, 35.051297
Ngimu	11	-4.745689, 35.051408
Ngimu	12	-4.749596, 35.049191
Ngimu	13	-4.747684, 35.053152
Ngimu	14	-4.776456, 35.054431
Ngimu	15	-4.774302, 35.058872
Ngimu	16	-4.777239, 35.062521
Ngimu	17	-4.770492, 35.098857
Ngimu	18	-4.769862, 35.097982
Ngimu	19	-4.752373, 35.098618
Ngimu	20	-4.751864, 35.098159
Ngimu	21	-4.749984, 35.098305
Ngimu	22	-4.750288, 35.098159
Ngimu	23	-4.748706, 35.098482
Ngimu	24	-4.744335, 35.096227
Ngimu	25	-4.743300, 35.098777
Ngimu	26	-4.739892, 35.094298
Ngimu	27	-4.738098, 35.093610
Ngimu	28	-4.739871, 35.069305

Ngimu	29	-4.739965, 35.068147
Ngimu	30	-4.742143, 35.066379
Ngimu	31	-4.744647, 35.063678
Ngimu	32	-4.745146, 35.062177
Ngimu	33	-4.746732, 35.058626
Ngimu	34	-4.752321, 35.058605
Ngimu	35	-4.763189, 35.055345
Ngimu	36	-4.764671, 35.056221
Ngimu	37	-4.768023, 35.061858
Ngimu	38	-4.775670, 35.061725
Ngimu	39	-4.772788, 35.063095
Ngimu	40	-4.772103, 35.064742
Ngimu	41	-4.775995, 35.087786
Ngimu	42	-4.756731, 35.092312
Ngimu	43	-4.756246, 35.083235
Ngimu	44	-4.758337, 35.075756
Ngimu	45	-4.764557, 35.072587
Ngimu	46	-4.756634, 35.077007
Ngimu	47	-4.770805, 35.092500
Ngimu	48	-4.764273, 35.089136
Mvae	1	-4.601437, 34.958812
Mvae	2	-4.600596, 34.955588
Mvae	3	-4.604946, 34.954837
Mvae	4	-4.606720, 34.954328
Mvae	5	-4.600458, 34.951520
Mvae	6	-4.601557, 34.951400
Mvae	7	-4.603469, 34.950788
Mvae	8	-4.606572, 34.948435
Mvae	9	-4.606840, 34.949195
Mvae	10	-4.603644, 34.947480
Mvae	11	-4.603561, 34.948759
Mvae	12	-4.602979, 34.947443
Mvae	13	-4.604217, 34.944441
Mvae	14	-4.611106, 34.937557
Mvae	15	-4.612695, 34.934805
Mvae	16	-4.624304, 34.931322
Mvae	17	-4.647437, 34.941958
Mvae	18	-4.632357, 34.979687
Mvae	19	-4.631821, 34.983940
Mvae	20	-4.625735, 34.982263
Mvae	21	-4.624405, 34.984431
Mvae	22	-4.618167, 34.981229
Mvae	23	-4.616200, 34.981063
Mvae	24	-4.613632, 34.980896

Mvae	25	-4.613558, 34.980683
Mvae	26	-4.612709, 34.976449
Mvae	27	-4.612459, 34.976245
Mvae	28	-4.607010, 34.973762
Mvae	29	-4.603021, 34.966081
Mvae	30	-4.602845, 34.966192
Mvae	31	-4.602384, 34.960030
Mvae	32	-4.602891, 34.959011
Mvae	33	-4.612025, 34.957232
Mvae	34	-4.612561, 34.955981
Mvae	35	-4.613614, 34.945891
Mvae	36	-4.614436, 34.945725
Mvae	37	-4.631678, 34.942158
Mvae	38	-4.633479, 34.940749
Mvae	39	-4.635316, 34.942630
Mvae	40	-4.636480, 34.939786
Mvae	41	-4.637570, 34.941639
Mvae	42	-4.639260, 34.941704
Mvae	43	-4.646583, 34.962402
Mvae	44	-4.644561, 34.968990
Mvae	45	-4.641255, 34.969351
Mvae	46	-4.639638, 34.969805
Mvae	47	-4.629798, 34.978505
Mvae	48	-4.627305, 34.978584
Mvae	49	-4.621575, 34.976398
Mvae	50	-4.617049, 34.956384
Mvae	51	-4.618635, 34.947411
Mvae	52	-4.624784, 34.949322
Mvae	53	-4.621561, 34.947330
Mvae	54	-4.633329, 34.945623
Mvae	55	-4.636372, 34.952022
Mvae	56	-4.639562, 34.948445
Mvae	57	-4.637484, 34.951341
Mvae	58	-4.639982, 34.952981
Mvae	59	-4.639498, 34.953685
Mvae	60	-4.636852, 34.955654
Mvae	61	-4.636639, 34.958090
Mvae	62	-4.637124, 34.961801
Mvae	63	-4.636085, 34.965998
Mvae	64	-4.625343, 34.965070
Mvae	65	-4.625229, 34.965081
Mvae	66	-4.622976, 34.965901
Mvae	67	-4.621304, 34.968287
Mvae	68	-4.620810, 34.961454

Mvae	69	-4.629394, 34.953520
Mvae	70	-4.631512, 34.952520
Mvae	71	-4.633264, 34.956318
Mvae	72	-4.632890, 34.961088
Mvae	73	-4.631846, 34.960050
Mvae	74	-4.629611, 34.963001
Mvae	75	-4.626615, 34.959378
1Mtinko	1	-4.519852, 34.811638
1Mtinko	2	-4.520423, 34.809261
1Mtinko	3	-4.520613, 34.808454
1Mtinko	4	-4.521140, 34.805960
1Mtinko	5	-4.521169, 34.805784
1Mtinko	6	-4.520832, 34.805652
1Mtinko	7	-4.521081, 34.805417
1Mtinko	8	-4.520774, 34.805124
1Mtinko	9	-4.521300, 34.805153
1Mtinko	10	-4.521213, 34.804640
1Mtinko	11	-4.522953, 34.804067
1Mtinko	12	-4.519311, 34.803422
1Mtinko	13	-4.519267, 34.803231
1Mtinko	14	-4.519194, 34.802674
1Mtinko	15	-4.519267, 34.801133
1Mtinko	16	-4.519297, 34.799446
1Mtinko	17	-4.512364, 34.803260
2Mtinko	1	-4.515378, 34.831683
2Mtinko	2	-4.515273, 34.831082
2Mtinko	3	-4.521114, 34.833892
2Mtinko	4	-4.521324, 34.834027
2Mtinko	5	-4.521054, 34.833411
2Mtinko	6	-4.521489, 34.833471
2Mtinko	7	-4.518448, 34.826245
2Mtinko	8	-4.518853, 34.825809
2Mtinko	9	-4.517475, 34.825809
2Mtinko	10	-4.516022, 34.825073
2Mtinko	11	-4.510061, 34.823285
3Tutu	1	-4.306567, 34.479063
3Tutu	2	-4.309521, 34.478909
3Tutu	3	-4.309969, 34.483935
3Tutu	4	-4.308681, 34.488952
3Tutu	5	-4.308373, 34.491853
3Tutu	6	-4.307794, 34.493463
3Tutu	7	-4.311900, 34.490196
3Tutu	8	-4.312264, 34.484600
3Tutu	9	-4.312264, 34.483065

3Tutu	10	-4.312899, 34.483514
3Tutu	11	-4.313468, 34.483580
3Tutu	12	-4.313898, 34.487005
3Tutu	13	-4.313888, 34.487417
3Tutu	14	-4.314318, 34.487398
3Tutu	15	-4.314224, 34.486893
3Tutu	16	-4.314304, 34.486883
3Tutu	17	-4.315157, 34.486312
3Tutu	18	-4.315988, 34.486336
3Tutu	19	-4.315521, 34.484698
3Tutu	20	-4.316091, 34.482990
3Tutu	21	-4.317712, 34.487313
3Tutu	22	-4.317709, 34.487218
3Tutu	23	-4.317760, 34.487169
4Mtinko	1	-4.519857, 34.811620
4Mtinko	2	-4.520439, 34.809262
4Mtinko	3	-4.520628, 34.808476
4Mtinko	4	-4.521153, 34.805928
4Mtinko	5	-4.521146, 34.805808
4Mtinko	6	-4.520843, 34.805630
4Mtinko	7	-4.520780, 34.805149
4Mtinko	8	-4.521077, 34.805440
4Mtinko	9	-4.521311, 34.805174
4Mtinko	10	-4.521222, 34.804699
4Mtinko	11	-4.519289, 34.803450
4Mtinko	12	-4.519301, 34.803247
4Mtinko	13	-4.519232, 34.802715
4Mtinko	14	-4.519263, 34.801162
4Mtinko	15	-4.519263, 34.799463
4Mtinko	16	-4.522941, 34.804115
4Mtinko	17	-4.524040, 34.807437
4Mtinko	18	-4.526820, 34.807551
4Mtinko	19	-4.527515, 34.807614
4Mtinko	20	-4.527376, 34.808527
4Mtinko	21	-4.529158, 34.805839